Preliminary assessment of FY-3D microwave instruments towards their use in NWP systems

Forecasting Research Technical Report 634

January 2019

Fabien Carminati[1], Nigel Atkinson[1], and Qifeng Lu[2]

[1] Met Office, Exeter EX1 3PB, UK

[2] National Satellite Meteorological Center, CMA, Beijing 100081, China

Met Office

Table of Contents

Abstract

This work presents the preliminary evaluation of the microwave instruments on board the latest Chinese polar platform, FY-3D. Comparing 24 hours of observations from the Microwave Temperature Sounder 2 (MWTS-2), the Microwave Humidity Sounder 2 (MWHS-2), and the Microwave radiation Imager (MWRI) to the Met Office short range forecasts, we have characterised instrumental biases, show how those biases have changed with respect to their predecessors on board FY-3C, and how they compare to Advanced Technology Microwave Sounder (ATMS) on board NOAA SNPP and Global Precipitation Measurement (GPM) Microwave Imager (GMI). MWTS-2 global biases are much reduced with respect to its predecessor and found within ± 1 K compared to ATMS at equivalent channel frequencies. A suboptimal averaging of raw digital counts is found to cause an increase in striping noise and a small though not negligible ascending-descending bias. MWHS-2 appears to have a new calibration improving the 183 GHz humidity channels with reduced biases with respect to the instrument on FY-3C and within ± 2.6 K to ATMS at equivalent channel frequencies. However, the 118 GHz channels present a cold bias compared to its predecessor, and the standard deviation of the background departure has increased a few tenths of Kelvin across all channels. MWRI presents the largest improvements with reduced global biases and standard deviation with respect to the FY-3C version. The 2 K solar-dependent bias that affects the instrument on FY-3C is reduced to 0.2 K or less for FY-3D MWRI. This instrument also compares well to GMI at 18, 23, and 89 GHz, but remains biased low at 10 and 36 GHz.

1. Introduction

Satellite microwave instruments have contributed to the Earth observing system for decades, providing key observations for numerical weather predictions (NWP), reanalyses, and climate data records (e.g. English et al., 2000; Uppala et al., 2005; Yang et al., 2016). Arguably of foremost importance, the assimilation of temperature, wind-derived, and humidity-sensitive microwave radiances have continuously driven the quality of weather forecasts at the Met Office and other NWP centres (Joo et al., 2013; Kazumori et al., 2016) leading to improved societal benefits and resilience to extreme weather events (Pielke and Carbone, 2002; Bauer et al., 2015).

Since the 1980's, China has developed extensive Earth observation satellite programmes dedicated to meteorology, oceanography, and Earth monitoring (Xingfa and Xudong, 2015) catching up in a field long dominated by the U.S. and Europe. Of particular interest to NWP centres, the FengYun-3 (FY-3) programme is composed of a fleet of two research and two operational platforms, FY-3A/B and FY-3C/D, respectively, and four more platforms are planned to be launched in the coming years (Yang et al., 2012). Note that FY-3A ceased operations in March 2018.

In this study, we focus on the Microwave Humidity Sounder 2 (MWHS-2) and the Microwave Temperature Sounder 2 (MWTS-2) instruments, first introduced as part of FY-3C payload and continued on FY-3D, as well as the Microwave Radiation Imager (MWRI) that has been part

of the payload of all FY-3 platforms to date. The instruments have radiometric capability in the 50-60 GHz oxygen band, in the 118 GHz oxygen and 183 GHz water vapour bands, and in the 10-89 GHz window frequencies, respectively, providing valuable information on temperature, humidity, and wind.

To date and to the best of our knowledge, only the China Meteorological Administration (CMA), Météo-France, the European Centre for Medium-Range Weather Forecasts (ECMWF), and the Met Office are operationally using observations from the microwave instruments on board the FY-3 constellation, although other major NWP centres are planning to investigate the use of those data.

Following the FY-3C power fault on May 2015 and the subsequent failure of MWTS-2, the instrument has never been used for operational purposes. However, Li and Liu (2016) have reported neutral to slightly positive impact on analyses and forecasts from a series of observing system experiments in CMA's global and regional assimilation and prediction system (GRAPES), in line with previous studies from Li and Zou (2014) and Li and Liu (2015) reporting similar impact from MWTS-1 (MWTS-2 predecessor on board FY-3A/B).

Observations from FY-3C MWHS-2 (and its less advanced predecessor FY-3B MWHS-1) have been assimilated in operations at the Met Office and ECMWF since 2016 (Chen et al., 2015, 2018; Carminati et al., 2018a, Lawrence et al., 2018), noting that at ECMWF, 118 and 183 GHz channels are assimilated in the all-sky framework, while only the 183GHz channels in clear sky are used at the Met Office. The impact was reported to be neutral to slightly positive at both centres. At the Met Office, MWHS-1 and MWHS-2 contribute to the total percentage impact on 24-h forecast error reduction by 0.8 and 1.5 %, respectively, as of August 2018.

There is no report of an operational use of MWRI, although observing system experiments are being carried out at the Met Office where it is envisaged to introduce the assimilation of MWRI observations in the operational system early 2019.

The microwave instruments on board FY-3D, the latest platform of the series launched on November 2017, are therefore expected to further improve and increase the resiliency of operational NWP systems. Following a successful post-launch test phase, CMA released a small 24-hour batch of observations from FY-3D MWTS-2, MWHS-2, and MWRI for the date of June 09, 2018, for initial evaluation. In line with the international effort to evaluate and optimise the use of data from the FY-3 programme for NWP applications, we investigate the data quality of this sample. This document is structured as follows: section 2 presents the instrument characteristics; the data quality is discussed in section 3; section 4 concludes the study.

2. Instrument characteristics

MWHS-2 is a 15-channel cross-track radiometer scanning a 2660 km swath in 98 steps at ± 53.35 ° from nadir. Its sounding capability covers the oxygen band at 118 GHz with a sub-satellite point resolution of 32 km, the water vapour band at 183 GHz with 16 km resolution, and window parts of the spectrum at 89 and 150 GHz with 32 km resolution. The five channels

dedicated to the 183 GHz band and sensitive to humidity, cloud, and precipitation, are similar although not identical to those of the Advanced Technology Microwave Sounder (ATMS) on board the NOAA SNPP and NOAA-20 platforms. The noise equivalent differential temperature (NEDT), a signal-to-noise measure of the instrument sensitivity used to estimate the random error in the observations, has been reported by Li et al. (2016) to be slightly larger than that of ATMS at equivalent channels. Unlike other space-borne radiometers, MWHS-2 also provides a unique insight into the 118 GHz band. While the three highest peaking channels near the band centre act as stratospheric temperature sounding channels, the sensitivity to cloud and precipitation – due to absorption, emission, and scattering from hydrometeors – increases with the distance to the band centre as the channels peak lower in the troposphere. Lawrence et al. (2017) showed that towards the edges of the band (at 118.75 ± 2.5 GHz), the absorption from the water vapour continuum is important compared to the absorption from dioxygen molecules in a dry atmosphere, which causes this channel to be also sensitive to water vapour. Finally, the two channels sounding the outmost edges of the band act as window channels with sensitivity to surface properties and water vapour. MWHS-2 characteristics are further detailed by Jieying et al. (2015) and table 1 summarizes the channel specifications along with those of ATMS.

Table 1: MWHS-2 and ATMS channel number, central frequency and polarization, bandwidth, horizontal resolution, and on-orbit NEDT.

Channel number		Central frequency (GHz) & polarization		Bandwidth (MHz)		Horizontal resolution (km)	
MWHS2	ATMS	MWHS2	ATMS	MWHS2	ATMS	MWHS2	ATMS
1	16	89.0 QH	88.2 QV	1500	2000	32	32
2	-	118.75 ± 0.08 QV	-	20	-	32	-
3	-	118.75 ± 0.2 QV	-	100	-	32	-
4	-	118.75 ± 0.3 QV	-	165	-	32	-
5	-	118.75 ± 0.8 QV	-	200	-	32	-
6	-	118.75 ± 1.1 QV	-	200	-	32	-
7	-	118.75 ± 2.5 QV	-	200	-	32	-
8	-	118.75 ± 3.0 QV	-	1000	-	32	-
9	-	118.75 ± 5.0 QV	-	2000	-	32	-
10	17	150 QH	165.5 QH	1500	3000	16	16
11	22	183.31 ± 1 QV	183.31 ± 1 QH	500	500	16	16
12	21	183.31 ± 1.8 QV	183.31 ± 1.8 QH	700	1000	16	16
13	20	183.31 ± 3.0 QV	183.31 ± 3.0 QH	1000	1000	16	16
14	19	183.31 ± 4.5 QV	183.31 ± 4.5 QH	2000	2000	16	16
15	18	183.31 ± 7.0 QV	183.31 ± 7.0 QH	2000	2000	16	16

QV = Quasi-Vertical QH = Quasi-Horizontal (i.e. polarization vector is parallel to the scan plane at nadir)

MWTS-2 is also a cross-track radiometer, it has 13 channels and covers a 2250 km swath in 90 steps with a sub-satellite point resolution of 32 km. In term of radiometric capability, MWTS-2 sounds the oxygen band between 50 and 60 GHz with sensitivity to temperature from the surface to the upper stratosphere. MWTS-2 channels also present similar characteristics to ATMS temperature-sensitive channels. FY-3C MWTS-2 NEDT is also slightly larger than that of ATMS according to Li et al. (2016). MWTS-2 is further detailed by Wang

and Li (2014) and table 2 summarizes the channel specifications along with ATMS equivalent channels.

MWRI is conical-scanning radiometer with an antenna diameter of 90 cm that provides Earth observations at a viewing angle of 53.1 ° in the forward direction ± 52 ◦ around the nadir for a total swath of 1400 km. In term of radiometric capability, MWRI has 10 channels with dual polarization at 10.65, 18.7, 23.8, 36.5, and 89.0 GHz. The spatial resolution ranges from 9 to 85 km, increasing with the decrease of frequency. The instrument is sensitive to surface thermal microwave emission and provides information on total column water vapour, cloud and precipitation, surface temperature, and surface wind over the ocean. MWRI benefits from an end-to-end 3-point calibration system involving three reflectors: a main reflector used for the Earth, cold and warm views, and two independent reflectors used for the cold and warm targets exclusively. This system allows to account for the emission contamination from the sun-heated main reflector in the on board calibration. MWRI characteristics, calibration system, and on orbit performances are further discussed by Yang et al. (2011), noting that the authors address on orbit performance of the instrument on FY-3A. It is worth noting that MWRI shares frequencies with other imagers, including the Global Precipitation Measurement (GPM) Microwave Imager (GMI), a state-of-the-art conical-scanning radiometer, which, according to the U.S. National Aeronautics and Space Administration (NASA), has achieved the highest standards of radiometric calibration and stability to date. Note that because the orbit pattern and antenna size (1.2 m) are different, GMI NEDT and ground resolution (see e.g. Newell et al., 2014) differ from MWRI. Table 3 summarizes MWRI and GMI channel specifications.

Table 2: Same as table 1 but for MWTS-2.

Channel number		Central frequency (GHz) & polarization		Bandwidth (MHz)		Horizontal resolution (km)	
MWTS2	ATMS	MWTS2	ATMS	MWTS2	ATMS	MWTS2	ATMS
1	3	50.30 QH		180	180	32	
2	4	51.76 QH		400	400	32	
3	5	52.80 QH		400	400	32	
4	6	53.596 ± 0.115 QH		400	170	32	
5	7	54.40 QH		400	400	32	
6	8	54.94 QH		400	400	32	
7	9	55.50 QH		330	330	32	
8	10	57.29 QH		330	155	32	
9	11	57.29 ± 0.217 QH		78	78	32	
10	12	57.29 ± 0.3222 ± 0.048 QH		36	36	32	
11	13	57.29 ± 0.3222 ± 0.022 QH		16	16	32	
12	14	57.29 ± 0.3222 ± 0.010 QH		8	8	32	
13	15	57.29 ± 0.3222 ± 0.0045 QH		3	3	32	

Table 3: MWRI and GMI channel number, central frequency and polarization, bandwidth, instantaneous field of view (IFOV), and on-orbit NEDT.

Channel number		Central frequency (GHz) & polarization		Bandwidth (MHz)		IFOV (km)	
MWRI	GMI	MWRI	GMI	MWRI	GMI	MWRI	GMI
1	1	10.65 V		180	96.5	51 x 85	19x32
2	2	10.65 H		180	94.7	51 x 85	19x32
3	3	18.7 V		200	193	30 x 50	11x18
4	4	18.7 H		200	194	30 x 50	11x18
5	5	23.8 V		400	367	27 x 45	10x16
6	-	23.8 H	-	400	-	27 x 45	-
7	6	36.5 V		400	697	18 x 30	9x15
8	7	36.5 H		400	707	18 x 30	9x15
9	8	89.0 V		3000	5470	9 x 15	4x7
10	9	89.0 H		3000	5516	9 x 15	4x7

V = Vertical H = Horizontal

3. Assessment

Upon reception, the data have been pre-processed with the ATOVS and AVHRR Preprocessing Package (AAPP[1]), converted to BUFR format, and stored in the Met Office observational database ready for use in the system. The pre-processing, in line with what was initially set up for FY-3C, consists in: a) the averaging of each three adjacent scan positions in order to avoid oversampling and b) the mapping of MWHS-2 to MWTS-2 observations with a median filter in brightness temperature that is applied to any MWHS-2 spots within 1.25 degree (in viewing angle) of each MWTS-2 spot. For MWRI, it was observed that the instrument on FY-3D has 266 fields of view (FOV) (compared to 254 on FY-3C), and was decided to discard the first and last 6 FOV and proceed with the 2-spots cross-track averaging already in place for FY-3C aiming to avoid over sampling and reduce the noise.

The assessment proposed here is based on the comparison between satellite observations and short-range forecasts from the Met Office global model, a proven methodology described by Saunders et al. (2013). NWP-based assessments have found a growing resonance with the improvement of model accuracy and have been successfully used for evaluation numerous satellite instruments, including from the FY-3 programme (e.g. Zou et al., 2011; Lu et al., 2011; Chen et al., 2015). The detection of fine complex biases in observation datasets is possible thanks to the high quality of NWP representation of atmospheric temperature and humidity that, when converted in the spectral domain, gives errors (uncertainties) estimated to be of the order of 0.1 K (0.1 K) at frequencies sensitive to mid-tropospheric and lower stratospheric temperature, and 0.5 K (2.5 K) at frequencies sensitive to mid and upper tropospheric humidity (Carminati et al., 2018b). At frequencies used by imager instruments, Carminati et al. (2017) highlighted biases of the order of 1 K.

To collocate observations and model fields, and quality control the data, FY-3D data have been processed in a clear-sky passive off-line mode of the Met Office observation processing

[1] https://nwpsaf.eu/site/software/aapp/

system (OPS). In operation, OPS acts as a low resolution N768L70 (~25 km at mid-latitudes, 70 levels from surface to 80 km) one-dimensional variational analysis (1D-Var) used to quality control and derive physical parameters for the subsequent main 4D variational process. The background used for the comparison and the 1D-Var retrieval is the short-range forecast from the previous assimilation cycle, interpolated at the observation location and time. The fast radiative transfer model RTTOV version 12 (Saunders et al., 2018) is used to map model variables in the observation spectral domain. Surface emissivity is calculated using FASTEM 2 (Kazumori and English, 2015) over oceans and an atlas is used over land (https://www.nwpsaf.eu/site/software/rttov/download/#Emissivity_BRDF_atlas_data, last accessed on January 7, 2019). The main assimilation system is a hybrid 4-dimensional variational analysis (4D-Var) with 6-hour time window with background error information provided by a low resolution global ensemble (Lorenc et al., 2000; Rawlins et al., 2007).
Because FY-3D data are used passively (i.e. they are not assimilated in 4D-Var), the background used for the comparison is therefore independent from the observations. On the contrary, ATMS, MWHS-2, and GMI are actively assimilated into the system, resulting in analyses and subsequent forecasts constrained by the value of their observations (depending on the weight given to the observations errors). As a consequence, the difference between observations and model background should be lower for the assimilated instruments than the difference between observations from FY-3D and model background.

In addition to background departure analyses (i.e. the difference observation minus background, hereafter O-B), we investigate the double difference with instruments of equivalent radiometric capability. FY-3D MWTS-2 and MWHS-2 are compared to SNPP ATMS equivalent channels and FY-3C MWHS-2 (FY-3C MWTS-2 data are not available on June 09, 2018), and FY-3D MWRI is compared to GPM GMI equivalent channels and FY-3C MWRI.
For this assessment, data are analysed before bias correction. OPS standard quality controls are applied to all observations and consist in a gross error check on the coordinates and the background, a convergence check, a radiative transfer error check, and a check on retrieved brightness temperature. Note that in operation, checks on observation brightness temperature and background departure are also conducted but were excluded from this analysis in order to evaluate the entire range of observations (and not only the “good ones”).
Two cloud tests are applied to MWTS-2 and MWHS-2 contemporaneously thanks to the mapping of both instruments. First, a maximum likelihood method, described by English et al. (1999), combines the first iteration of the 1D-Var based on observations at 183 ± 7, 183 ± 3 and 183 ± 1 GHz and an imposed threshold on the magnitude of the background departure at 183 ± 7 GHz. Second, a scattering test is based on the difference in brightness temperature at 89 and 150 GHz (and an index calculated as a function of the satellite zenith angle) and is described by Bennartz et al. (2002). For MWRI, a threshold imposed on the liquid water path retrieved in 1D-Var is set to 10 $g.m^{-2}$ and all observations with O-B greater than 4.3 K at 36.6 GHz (H) are marked as cloudy.
ATMS benefits from the same cloud tests as the block MWTS-2 + MWHS-2. GMI benefits from the same tests as MWRI but also has an additional quality control based on the quality flag provided by NASA (this includes, for example, observations contaminated by radio frequency interference).

MWHS-2 and MWRI observations (and ATMS and GMI equivalent) are considered over ocean only, while MWTS-2 observations (and ATMS equivalent) over ocean and land. High land (1000 m above sea level) and sea ice are excluded for all instruments.
The results are discussed below.

a) MWTS-2

Global O-B values have been calculated for FY-3D MWTS-2 and compared to ATMS at equivalent channel frequencies. Figure 1 shows the resulting mean, median and standard deviation for both instruments on June 09, 2018. MWTS-2 mean biases ranges -1.3 to 0.5 K depending the channel. It is worth noting that those values are up to an order of magnitude smaller than the mean biases found for the instrument on FY-3C evaluated by Lu et al. (2015). FY-3D MWTS-2 and ATMS instruments have a consistent bias both is sign and magnitude with differences in the mean not exceeding ± 0.5 K in most channels. Only channel 1 (50.3 GHz) and channel 5 (54.4 GHz) present a larger difference reaching 0.8 and 1 K, respectively.

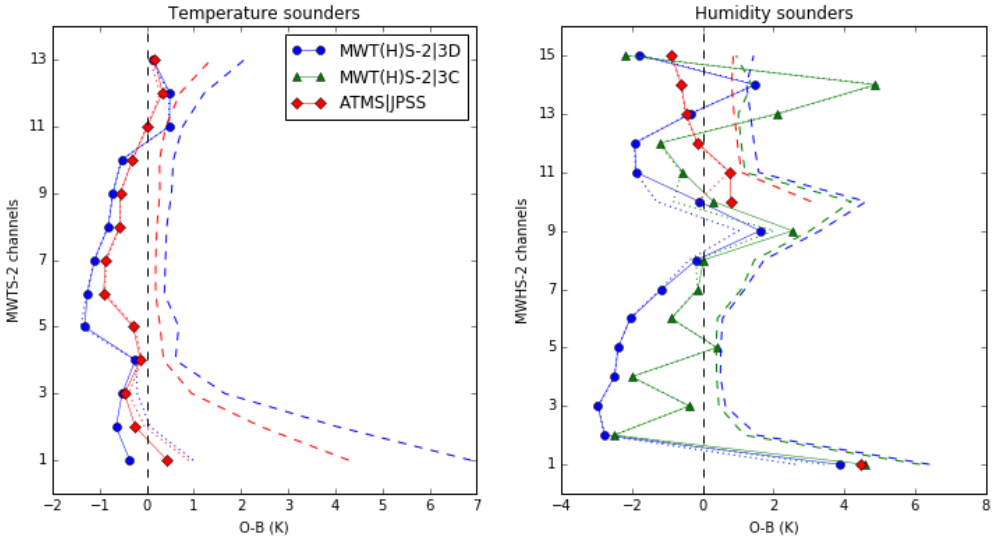

Figure 1: (Left) FY-3D MWTS-2 (blue) and SNPP ATMS (red) clear-sky sea and land O-B for June 09, 2018. Solid lines show the mean, dotted lines the median, and dashed lines the standard deviation. (Right) Same as left but for FY-3D MWHS-2 (blue), FY-3C MWHS-2 (green), and SNPP ATMS (red) over sea only.

For channel 1, this difference can be explained by a greater number of observations along the coasts of Antarctica and Greenland (see e.g. on figure 2) compared to ATMS. The O-B at low surface-sensitive frequencies in those regions are characterised by large negative biases, mostly due to the misrepresentation of surface emissivity in the NWP model, and the difference with ATMS can be explained by a greater number of data passing the quality control in MWTS-2 data set, possibly due to a misinterpretation of surface type in the 1D-Var step. The nearly identical median further confirm that the difference in the mean is largely

due to outliers. Those outliers are not expected to have an impact in the future use of the data as most will be removed by the background departure check, omitted in this study.

For channel 5 however, both mean and median consistently show a clear distinction between MWTS-2 and ATMS. Furthermore, the channel peaks in the mid-troposphere and has low sensitivity to the surface, meaning that the difference cannot be explained by the polar outliers. The O-B anomaly (i.e. O-B minus mean(O-B)) shown on figure 2 reveals that channel 5 is strongly affected by a scan bias of up to 2 K edge-to-edge. Although channel 5 is the most affected, large bias variations, greater than 1 K, along the scan line are also visible in channels 1-6, as shown on figure 3, associated in some instances with complex patterns. Note that on figure 3, scan positions range from 1 to 30 because of the pre-processing step that averages one in three scan positions. Scan-dependent biases have been previously reported for the MWTS-2 instrument on board FY-3C (Lu et al., 2015; Li et al., 2016; Tian et al., 2018). As suggested by Lu et al. (2015), a contamination of the antenna by the cold target could lead to lower-than-normal observed Earth temperature and subsequent cold bias in the O-B. This hypothesis is consistent with the bias patterns observed in channels 1-8 in fig. 3 that consistently shows negative O-B strengthening from scan position 1 to 22. For some channels, the bias stabilizes, if not slightly recovers, over the last six scan positions, possibly thanks to the antenna pattern correction. Although the root of the problem will have to be addressed through a revised antenna correction in the calibration system, bias corrections in place at the Met Office, ECMWF, or CMA were shown to efficiently remove the most detrimental effects (Lu et al., 2015; Li et al., 2016).

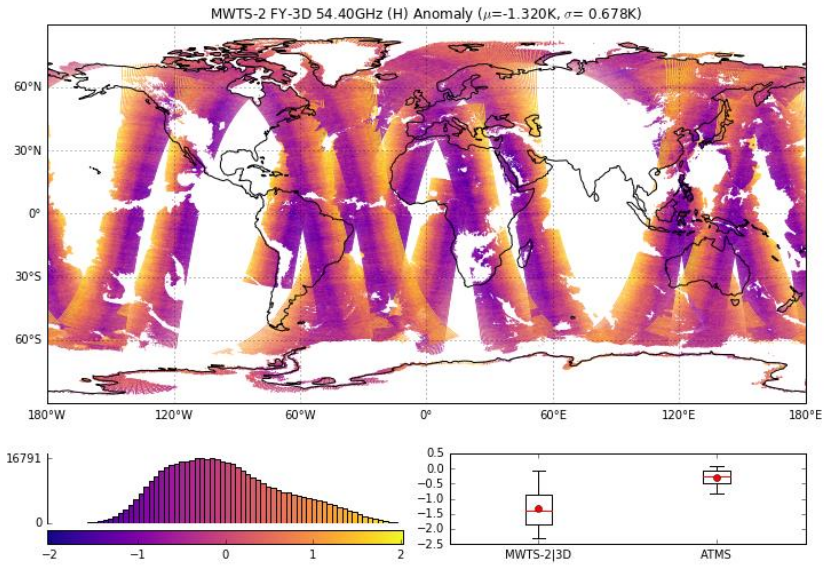

Figure 2: FY-3D MWTS-2 channel 5 (54.4 GHz) anomaly on June 09, 2018. The boxplots show, for FY-3D MWTS-2 and SNPP ATMS, the O-B lower to upper quartile, the whiskers reach 5 and 95%, the red line shows the median and the red dot the mean.

In their assessment of FY-3C MWTS-2, Lu et al. (2015) also highlighted a dependence of the bias on scene temperature. This may happen when the observed temperature deviates from

the linear assumption used for the interpolation of digital counts from cold to warm targets. This effect is generally removed by applying a non-linearity correction in the calibration. In some instances however, the correction is not optimized as shown by Atkinson et al. (2015) for FY-3C MWTS-2. In order to investigate if such a dependency can be found in the FY-3D MWTS-2 data set, we analysed the O-B as a function of the background scene temperature as in figure 4 (left) and calculated the slope and correlation of a linear least-squares regression as reported in table 4 along with those of ATMS for comparison. It must be noted that the regression uses all the available data which can result in an overall flatter slope compared to one that would use only the most densely populated region of temperature (e.g. between 210 and 230 K on figure 4). This caveat should disappear when a larger sample (e.g. several months of data) will be available to analyse. Note that surface sensitive channels are omitted from this analysis in order to avoid model-based biases related to surface emissivity being entangled with instrument biases. The slopes (correlations) are found to range from -0.041 $K.K^{-1}$ (-0.36) at 54.4 GHz (MWTS-2 channels 5) to 0.001 $K.K^{-1}$ (0.01) at 57.29 ± 0.322 ± 0.048 GHz (MWTS-2 channel 10). They are of the same order as for ATMS, although sometimes of opposite sign (i.e. at 54.4, 54.94, and 57.29 ± 0.322 ± 0.022 GHz).

Additionally, Lu et al. (2015) detected in some FY-3C MWTS-2 upper atmosphere channels a land-sea contrasts. The problem was suspected to be caused by inter-channel interferences but this has not been seen in the FY-3D data set.

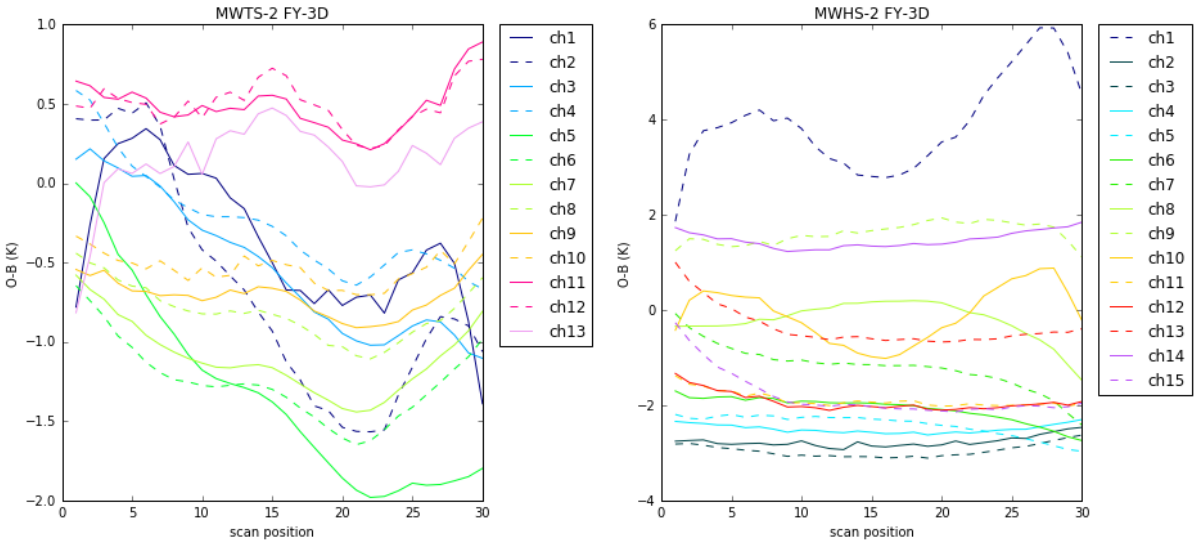

Figure 3: (Left) FY-3D MWTS-2 O-B on June 09, 2018, per channel in function of the scan position. (Right) Same as left but for FY-3D MWHS-2.

Biases along the satellite orbit are also investigated as shown on figure 4 (right). O-B are analysed as a function of orbital angle, the angle around the orbital track, relative to the intersection of the satellite ascending node with the ecliptic plane. In this coordinate system, the satellite is over the equator on the ascending node at 0 °, over the North Pole at around 90 °, over the equator on descending node at 180 °, and over the South Pole around 270 °.

While channels 1-3 are found relatively insensitive to changes in orbital angle, the higher frequency channels generally present peaks near the polar latitudes. This is characteristic to air mass dependent biases that translate into positive anomalies at high latitudes and to negative anomaly in the tropics. This pattern is not seen in channels 8 and 11 that instead have a cold bias over the Southern ocean only (not shown). Another interesting feature is a local maximum that appears between 120 ° and 150 ° (mid-northern latitudes descending node), detected in channels 4-11 (the signal being too noisy to conclude for channels 12-13). Given the reduced amount of data, this feature is potentially an artefact due to a sampling effect or may result from a large scale weather pattern. It will be interesting to monitor the persistence of the feature in this segment of the orbital angle over several months when the data become available. The orbital-based analysis additionally gives insight into any discrepancies between data from the ascending and descending nodes. We found no significant difference between ascending and descending passes in FY-3D MWTS-2 channels apart from channels 12 and 13 that present a 0.2 and 0.5 K bias, respectively (not shown). This bias is likely related to a calibration issue discussed further below.

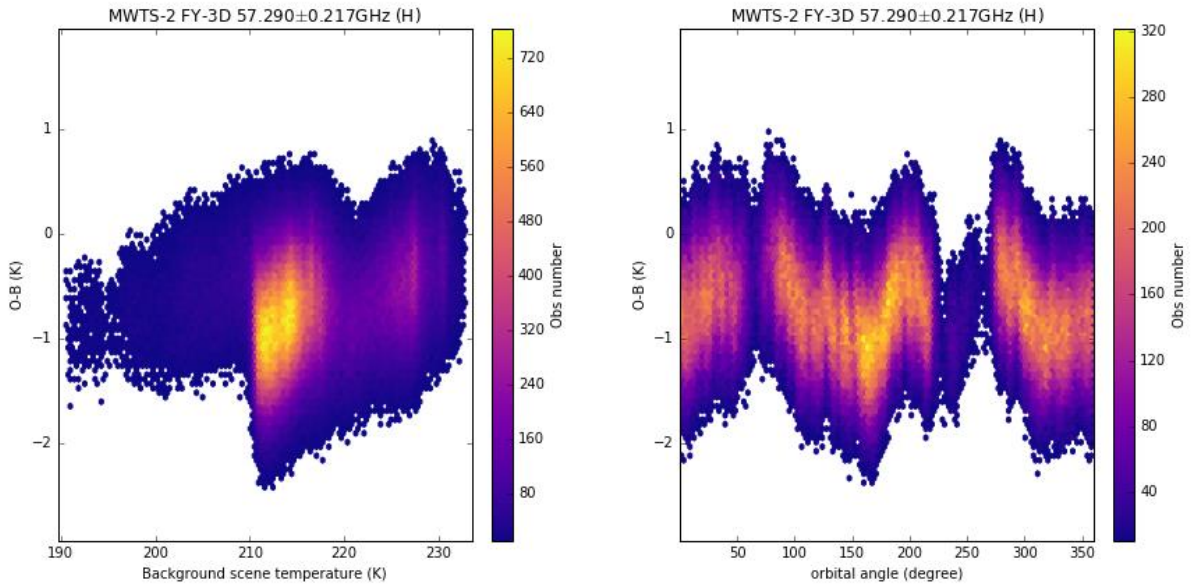

Figure 4: (Left) FY-3D MWTS-2 channel 9 (57.29 ± 0.217 GHz) O-B in function of the background scene temperature. (Right) FY-3D MWTS-2 channel 9 O-B in function of the platform orbital angle[2]. The colour bars indicate the number of observations.

[2] See Booton et al. (2014)

Table 4: Slope, intercept, and correlation coefficient from a linear least-squares regression between the background scene temperature and FY-3D MWTS-2 (SNPP ATMS) O-B.

Frequency [GHz]	Slope [$K.K^{-1}$] (MWTS-2_{3D} / ATMS)	Intercept [K] (MWTS-2_{3D} / ATMS)	r-value (MWTS-2_{3D} / ATMS)
54.40	-0.041 / 0.023	8.50 / -5.89	-0.36 / 0.49
54.94	-0.027 / 0.008	5.04 / -2.73	-0.34 / 0.19
55.50	0.002 / 0.007	-1.69 / -2.55	0.03 / 0.21
57.29	0.009 / 0.009	-2.88 / -2.61	0.17/ 0.32
57.29 ± 0.217	0.015 / 0.008	-3.96 / -2.45	0.19/ 0.20
57.29 ± 0.322 ± 0.048	0.001 / 0.001	-0.67 / -0.66	0.01 / 0.04
57.29 ± 0.322 ± 0.022	0.010 / -0.006	-1.84 / 1.59	0.15 / -0.19
57.29 ± 0.322 ± 0.01	-0.007 / -0.014	2.32 / 3.75	-0.08 / -0.27
57.29 ± 0.322 ± 0.0045	-0.035 / -0.040	8.85 / 10.2	-0.23 / -0.42

Ignoring window channels impacted by surface type and emissivity, FY-3D MWTS-2 O-B standard deviation ranges between 0.3 and 0.8 K for channels 4-11, systematically 0.2-0.4 K larger than that of ATMS at equivalent frequencies. For channels 12 and 13 the standard deviation increases up to 2 K along with the difference with ATMS that reaches up to 0.7 K (fig. 1). The increase of standard deviation difference between the two instruments for channels 12 and 13 is consistent with the ascending-descending bias affecting MWTS-2.

Also contributing to the instrument noise, a cross-track disturbance, known as striping noise, has been detected in channels 4-13. Striping, also identified in ATMS temperature sounding channels, is the result of gain fluctuations in the instrument amplifier used in the calibration system (Bormann et al., 2013). Both Li et al. (2016) and Lu et al. (2015) have noted striping in FY-3C MWTS-2 data set. Li et al. (2016) calculated that FY-3C MWTS-2 striping affects all channels and ranges from 0.1 to 0.7 K in term of standard deviation, noting that the striping pattern are not visible when the standard deviation in O-B is significantly larger. Here, we characterise this striping noise with the same index as presented by Lu et al (2015) that is, the ratio of along-track to cross-track variability. The indexes, shown in table 5, are generally larger than for ATMS on S-NPP, which has striping ratios varying between 1.0 and 1.6 in the temperature-sounding channels, but reduced compared to MWTS2 on FY-3C.

Table 5: Striping index calculated as the root-mean-square of the ratio of the along-track standard deviation to the cross-track standard deviation of the calibration view samples grouped into boxes of 8 pixels by 8 scans.

channel	1	2	3	4	5	6	7	8	9	10	11	12	13
Striping index	2.78	2.43	2.50	2.23	2.16	1.77	2.22	1.85	1.69	1.88	1.53	1.90	1.68

FY-3D MWTS-2 NEDT is shown in table 6. It is computed from the warm calibration counts as the standard deviation of the difference between warm counts and a rolling average over 7 lines but excluding the line under test. The standard deviation of the counts differences is then normalised by the channel gain. FY-3D MWTS-2 NEDT are similar or smaller to that reported by Lu et al. (2015) for FY-3C MWTS-2. It is also smaller than ATMS, noting however

that the on-board processing is different and the time interval between scans (and hence the integration time) is longer for MWTS-2.

In addition it is worth noting that there are significant correlations between FY-3D MWTS-2 adjacent samples in the calibration views, presumably due to the characteristics of the electronic filtering.

Table 6: Estimated FY-3D MWTS-2 NEDT from the warm calibration counts of the on board computer files.

channel	1	2	3	4	5	6	7	8	9	10	11	12	13
NEDT (K)	0.25	0.17	0.17	0.18	0.17	0.18	0.21	0.30	0.39	0.42	0.56	0.87	1.33

Investigating the source of the ascending-descending bias detected in channels 12 and 13, we used the instrument raw digital counts (i.e. level 0) form the on board computer (OBC) files to derive the antenna temperature and compare it to the reported temperature. As a first step, we averaged the raw counts across scan lines using a triangular function of total width 7 scan lines and compared it with that of CMA. As shown on figure 5, our averaging follows the raw data, while CMA averaging is shifted by a few scan lines. Such a displacement is consistent with the algorithm originally used on FY-3C that was used to replace all points outside one standard deviation away from the mean with the mean value of the 20 following samples. It was then argued that the averaging should instead use three standard deviation as threshold to filter outliers and the outliers replaced by a mean centred on its position (instead of being based on the following points). A correction was later applied to FY-3C. Our results suggests that FY-3D algorithm is similar to the original pre-correction algorithm used on FY-3C.

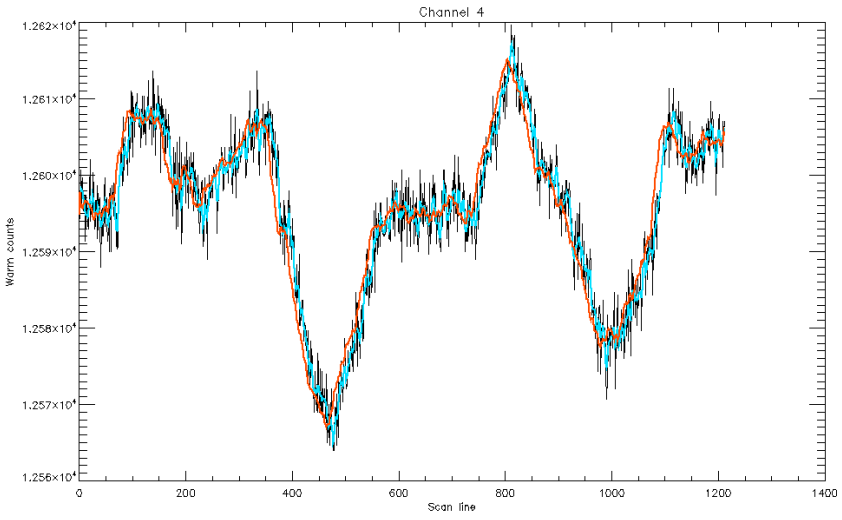

Figure 5: Averaging of the warm calibration counts MWTS-2 FY-3D channel 4. Raw data are shown in black, CMA averaging in red, and Met Office averaging in blue.

Using the Met Office averaged raw counts we derived the antenna temperature with a linear calibration as in Atkinson et al. (2015) and compared it to CMA antenna temperature as shown in figure 6. The difference between Met Office and CMA antenna temperature reveals that the current algorithm used by CMA causes the temperature to be locally up to 2 K warmer than that of the Met Office on the ascending node, and conversely 2 K colder on the descending node explaining the observed ascending–descending bias. Note that although this is found to be a major source of bias for channels 12 and 13, the impact is minor for lower frequency channels with respect to the dominant scan bias. However, the cross-scan bias patterns visible on figure 6 also suggest a significant effect on the striping nose. It is therefore recommended that CMA implements a similar correction as the one used on FY-3C for FY-3D MWTS-2 calibration system since a shift of average raw counts causes biases the derived antenna temperature and ultimately systematic errors in level 1 brightness temperature.

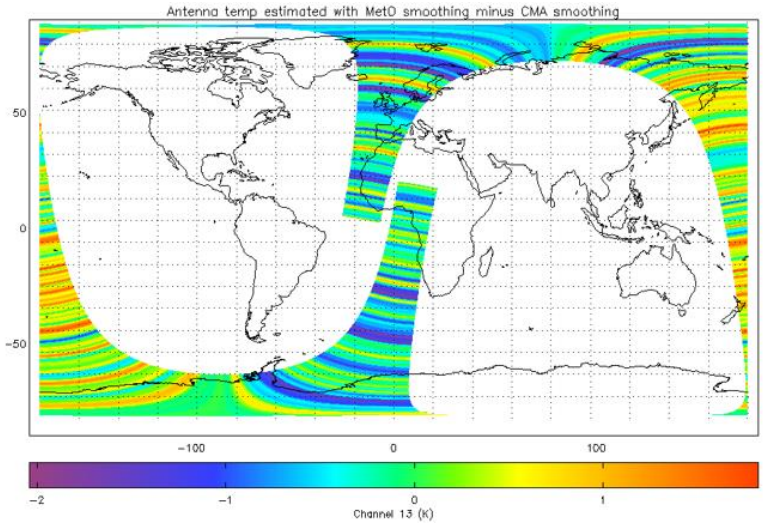

Figure 6: FY-3D MWTS-2 Met Office-derived minus original antenna temperature (channel 13).

b) MWHS-2

The global mean O-B over ocean has been calculated for FY-3D and FY-3C MWHS-2, and ATMS at equivalent channel frequencies (fig. 1, right). FY-3D MWHS-2 has a bias pattern comparable to that of FY-3C albeit shifted (to various extent depending on the channel) towards negative values. In the 183 GHz channels, FY-3D MWHS-2 O-B range from -1.9 to 1.4 K compared to -1.2 – 4.8 K for the instrument on FY-3C. Compared to ATMS, the O-B are found within ± 2.6 K, noting that ATMS O-B at 183.31 ± 3 and ± 4.5 GHz (MWHS-2 channel 13 and 14, respectively) does not exhibit a positive peak like the MWHS-2 instruments. This difference was also noted by Lawrence et al. (2018) who compared FY-3C MWHS-2 to ATMS and the Microwave Humidity Sounder (MHS) on board various U.S. and European platforms. The authors pointed out that while the biases at 183 GHz are consistent amongst most microwave instruments

and could be related to biases in radiative transfer modelling of this humidity band (Brogniez et al., 2016; Calbet et al., 2018), the different pattern observed for FY-3C MWHS-2 is more likely to be an instrument-related bias. The hypothesis of instrument-related bias is further supported by the similar bias found on FY-3D MWHS-2 that has the same design and characteristics as its predecessor. The shift in O-B between the two MWHS-2 is likely attributed to different pre-launch calibration set up, including the correction of biases from the warm and cold targets, the derivation of coefficients for the nonlinearity correction, and the correction for channels breaking the monochromatic assumption, that have been derived using a new thermal vacuum test facility as described by Wang et al. (2018). It is worth noting that in their study, the authors found that FY-3D MWHS-2 channel 14 is affected by a radiation leakage originating from the receiver used for the high frequency channels (150 and 183 GHz). The antenna leak radiation that bounced back from the device surrounding unless covered with a black body absorber. The authors concluded that this should not impact operational performances since there is no surrounding in space. However, both Lawrence et al. (2017, 2018) and Carminati et al. (2018a) noted that FY-3C MWHS-2 channels 13 and 14 have been experiencing large bias shifts and drifts that were found strongly correlated with the instrument environment temperature. Implications are that the sensitivity of those channels to temperature changes may be related to the leakage highlighted by Wang et al. (2018) through contamination by the radiation directly emitted by the platform, or by the antenna emission interacting with the body of the platform, or a combination of both.

In the 118 GHz channels, the findings are similar. FY-3D MWHS-2 biases are shifted towards negative values (down to -3 K) compared to that of FY-3C. We can note however that FY-3D MWHS-2 bias reduces to nearly zero, relatively smoothly, from high peaking to low peaking channels (and become positive in the lowermost surface sensitive channel 9). Although this reduction of bias with the decrease of the height of sensitivity is also visible for FY-3C MWHS-2, the channel-to-channel variation in bias is more erratic.

The standard deviation of FY-3D MWHS-2 O-B is comparable to that of FY-3C and while systematically larger, the difference is nonetheless smaller than 0.5 K. Similarly, FY-3D MWHS-2 standard deviation is comparable although 0.4 to 0.6 K larger than that of ATMS at 183 GHz. We can note again that the large standard deviation in window channels is dominated by model error.

The variation of O-B with the scan position is also analysed for FY-3D MWHS-2 (fig. 3, right). Window channels 1 and 10 (89 and 150 GHz, respectively) present the distinctive double maxima with up to 4 K peak-to-peak amplitude, somewhat similar in shape to those of MWTS-2 window channel 1 and to a lesser extent channel 2 (50.3 and 51.76 GHz, respectively). Interestingly, the 118 GHz channel sensitive to surface (channels 8 and 9) do not present such pattern that seem to only affect channels with a QH polarization. The bias is relatively homogeneous and within 2 K amplitude across the other channels.

Li et al. (2016) also analysed FY-3C MWHS-2 striping noise and showed that it affects all channels with a standard deviation of up to 0.8 K, but again, the striping patterns are visible only when the standard deviation in O-B is small, e.g. at 118 GHz. Figure 7 shows an example of visible striping noise detected in FY-3D MWHS-2 channel 4 (118.75 ± 0.3 GHz). Visible striping is also present in channels 2-6. The striping index (and the NEDT) however could not be calculated due to missing on board computer files for the available sampling.

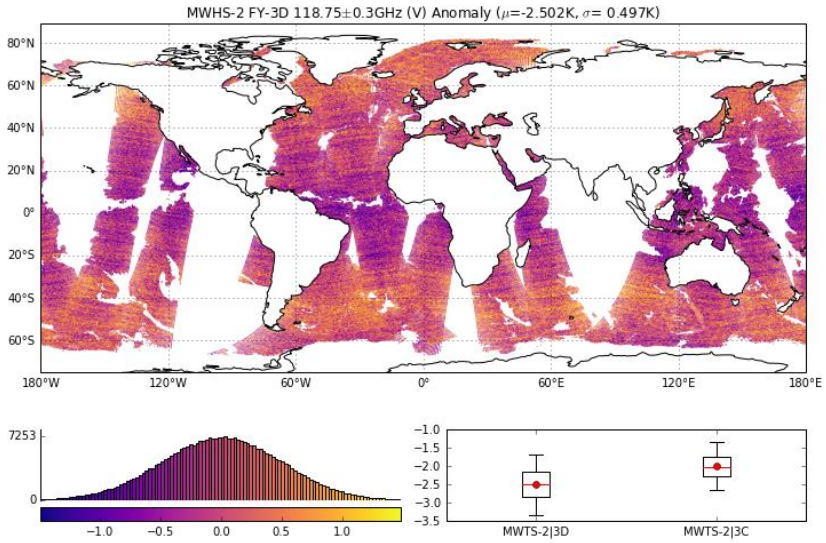

Figure 7: Same as figure 3 but for FY-3D MWHS-2 channel 4 (118.75 ± 0.3 GHz). The boxplot compares FY-3D MWHS-2 to FY-3C MWHS-2.

Figure 7 also reveals an example of air mass dependent bias with the tropics low biased with respect to high latitudes. Analyses of O-B in function of the orbital angle have also been carried out for FY-3D MWHS-2 (not shown). Two different regimes were detect: a) channels 3 and 4 (118.75 ± 0.2 and ± 0.3 GHz) are low biased in the tropics with respect to high latitudes and b) channels 5 and 6 (118.75 ± 0.8 and ± 1.1 GHz), and to a lesser extent 11 and 12 (183.31 ± 1 and ± 1.8 GHz), are low biased at high latitudes with respect to the tropics. Investigating the difference between ascending and descending nodes (ignoring window channels), we found O-B differences less than 0.1 K in the high peaking 118 GHz channels, rising to 0.7 K in channel 7 (118 ± 2.5 GHz). The 183 GHz channels are mostly unaffected (maximum difference of 0.1 K in channel 15).

Linear regressions of the O-B as a function of the scene temperature are calculated for FY-3D MWHS-2 channels 2-6 and 11-15 (with the same caveat as described for MWTS-2), and the slopes, intercepts, and correlation coefficients shown in table 7 along with those of FY-3C MWHS-2 and ATMS (at equivalent frequencies). Slopes are similar between the two MWHS-2 instruments in the 118 GHz channels and range from -0.054 to 0.031 $K.K^{-1}$ with correlation varying between -0.27 and 0.37 (for FY-3D MWHS-2). Interestingly, those results are of the same order as for the temperature channels sounding the 54-57 GHz oxygen band on MWTS-

2 (see table 4). In the 183 GHz channels, at the exception of the lowest peaking 183.31 ± 7 GHz that has a nil slope, the fits of FY-3D MWHS-2 O-B and scene temperature have slopes (correlations) ranging from -0.025 to 0.034 $K.K^{-1}$ (from -0.15 to 0.15), similar to those of FY-3C MWHS-2, but larger than those of ATMS virtually neutral. It must be noted however, that even a change of -0.025 $K.K^{-1}$ (FY-3D MWHS-2 at 183 ± 4.5 GHz) remains small compared to NWP model uncertainties that are up to 2.5 K at 183 GHz.

Table 7: Same as table 4 but for FY-3D MWHS-2.

Frequency [GHz]	Slope [$K.K^{-1}$] (MWHS-2_{3D} / MWHS-2_{3C} / ATMS)	Intercept [K] (MWHS-2_{3D} / MWHS-2_{3C} / ATMS)	r-value (MWHS-2_{3D} / MWHS-2_{3C} / ATMS)
118.75 ± 0.08	-0.054 / -0.029	9.16 / 4.09	-0.27 / -0.18
118.75 ± 0.2	0.031 / 0.021	-9.64 / -5.04	0.28 / 0.29
118.75 ± 0.3	0.030 / 0.032	-9.00 / -9.00	0.37 / 0.51
118.75 ± 0.8	0.012 / 0.008	-5.36 / -1.57	0.13 / 0.12
118.75 ± 1.1	0.020 / 0.033	-7.08 / -9.05	0.25 / 0.55
183 ± 1.0	0.034 / 0.013 / 0.008	-10.4 / -3.81 / -1.29	0.15 / 0.08 / 0.06
183 ± 1.8	0.024 / 0.011 / -0.003	-8.13 / -4.19 / 0.77	0.12 / 0.09 / -0.03
183 ± 3.0	-0.018 / 0.014 / -0.005	4.60 / -1.68 / 1.00	-0.10 / 0.11 / -0.05
183 ± 4.5	-0.025 / 0.062 / 0.002	8.33 / -11.8 / -1.28	-0.15 / 0.34 / 0.02
183 ± 7.0	0.001 / 0.019/ -0.011	-2.11 / -7.38 / 2.30	0.01 / 0.15 / -0.11

c) MWRI

MWRI on board FY-3C has been thoroughly evaluated by Lawrence et al. (2017). Here we evaluate the instrument on board FY-3D in the light of their findings and in comparison to FY-3C MWRI and GMI. Figure 8 shows the clear sky global mean, median, and standard deviation of O-B over ocean for all three instruments. Note that GMI does not have a 23.8 GHz channel with horizontal polarization (MWRI channel 6). Global biases are consistent in shape between the two MWRI instruments, though reduced on FY-3D by 0.4 to 1.1 K compared to FY-3C (expect channels 1 and 10). Compared to GMI, we can note the signs of the inter satellite bias already noted by Lawrence et al. (2017) with FY-3D MWRI 1.7 to 5.2 K low biased and O-B of opposite sign at 10 and 36 GHz (channels 1, 2, 7, and 8). However, this is not verified at 18, 23, and 89 (V) GHz (channels 3, 4, 5, and 9) where all instruments show consistent biases with difference between FY-3D MWRI and GMI less than 0.7 K. Although of same sign, the larger difference between FY-3D MWRI and GMI compared to FY-3C MWRI and GMI at 89 (H) GHz remains unexplained, but likely lies in the calibration of the instrument.

The standard deviation is systematically reduced, by up to 1.5 K, for FY-3D MWRI compared to the instrument on FY-3C, with the largest gain visible in the low frequencies. This is consistent with the correction applied by CMA (only to FY-3D MWRI to the best of our knowledge) to the warm target that used to suffer a contamination of the warm load view from the Earth scene affecting the warm reflector back lobe. This correction has been presented by Shengli Wu (National Satellite Meteorological Center of CMA) at the Global Space-based Inter-Calibration System (GSICS) meeting in Shanghai 2018[3]. It is also very

[3] http://gsics.atmos.umd.edu/bin/view/Development/20180319 (presentation 9b)

encouraging that FY-3D MWRI and GMI standard deviation are nearly identical at 36 and 89 GHz. The large difference (up to 4 K) observed between those two instruments at low frequency is explained by MWRI larger field of view (see table 3) that is contaminated by land surface in coastal areas.

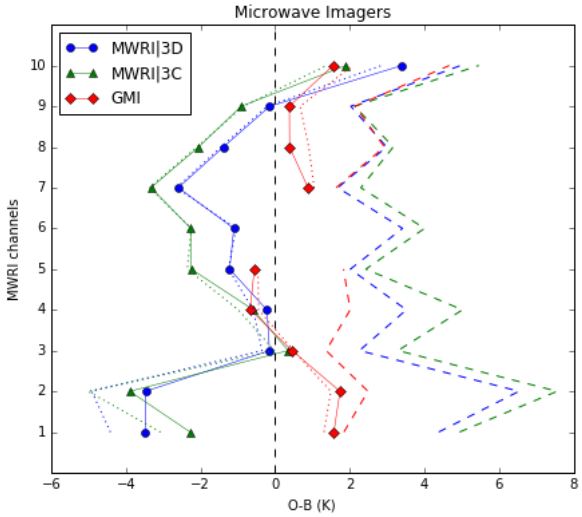

Figure 8: FY-3D MWRI (blue), FY-3C MWRI (green), and GPM GMI (red) O-B on June 09, 2018 in clear-sky condition over ocean. Solid lines show the mean, dotted lines the median, and dashed lines the standard deviation.

The foremost issue with FY-3C MWRI as highlighted by Lawrence et al. (2017) is a strong solar-dependent bias leading to difference between the ascending and descending node as large as 2 K and consistent across all channels. Such a bias, previously detected on legacy imagers (Bell et al., 2008; Geer et al., 2010) results from thermal emissions from sun-heated element(s) of the instrument (usually the main antenna) contaminating the received signal and unaccounted for in the calibration. MWRI 3-point calibration however compensates for any contamination from the main receiver, therefore Lawrence et al. (2017) suggested that the reflectors dedicated to the warm and cold targets (whose emission are unaccounted for in the calibration) may significantly contribute to the ascending-descending bias. Because such a bias is complex to understand and all the more difficult to correct in the context of NWP systems, MWRI observations have not been used in data assimilation systems. It is worth noting however that a correction is being tested for potential assimilation at the Met Office (Carminati et al., 2018a).

At the Shanghai 2018 GSICS meeting, Shengli Wu also presented the details of an emissivity correction for the warm and cold reflectors (same presentation as above) and claimed to have reduced the ascending-descending bias to less than 0.1 K. To investigate this point, we compare in figure 9 FY-3D MWRI O-B for the ascending node only, for the descending node only, and their difference per channel (left) to that of FY-3C (right). The ascending-descending difference that range from 1.5 to 2.5 K for FY-3C MWRI is reduced to less than 0.7 K for FY-3D

MWRI. Furthermore, the largest differences for the instrument on FY-3D are obtained only for channel 1 and 2 (10.65 GHz), 0.6 and 0.7 K respectively, and may be the result of a sampling effect due to the small size of the analysed sample (e.g. one node might see more coastline than the other). When focusing on the higher frequency channels, the difference ranges from 0.003 to 0.2 K.

The successful removal of MWRI solar-dependent bias on FY-3D will have a significant impact for the future use of the instrument in NWP centres that will be able to assimilate its observations without having to implement complex bias corrections. It must be noted however that another feature highlighted by Lawrence et al. (2017) was the drift in time of FY-3C MWRI global bias (up to 2 K in four years) in parallel with the increase in amplitude of the solar-dependent bias, the latter potentially the cause of the former. Because the reflector emissivity correction applied by CMA is a one-time change, it will be important to closely monitor MWRI bias over time and apply an updated correction if a degradation is detected.

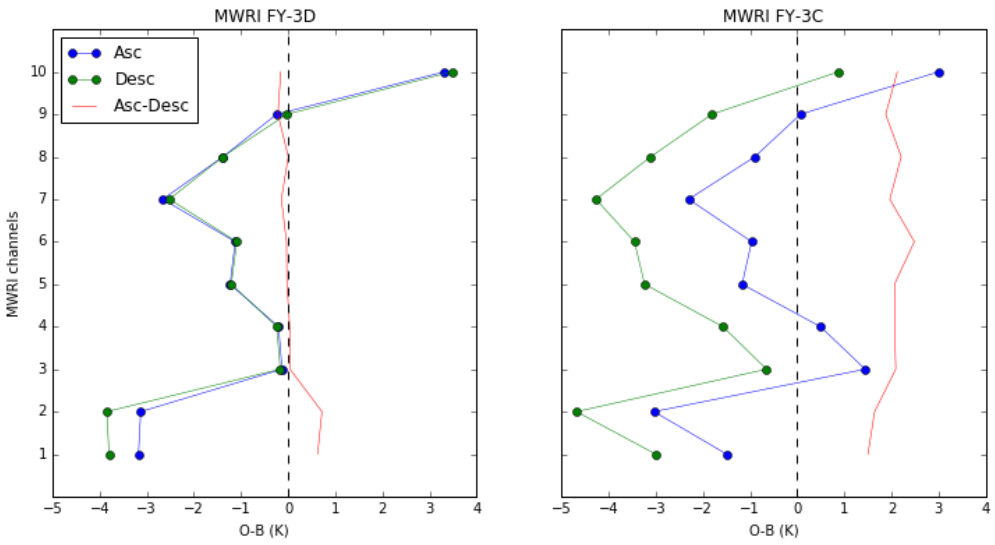

Figure 9: (left) FY-3D MWRI O-B from the ascending nodes (blue), from the descending nodes (green), and their difference (red) on June 09, 2018 in clear-sky condition over ocean. (Right) same as left but for FY-3C MWRI.

Finally, we can note that both Zou at al. (2012) and Lawrence et al. (2017) have reported radio frequency interferences (RFI) affecting MWRI on board FY-3B and FY-3C, but the small sampling size of our dataset does not allow the detection (with confidence) of RFI.

4. Conclusion

Following the launch of FY-3D, the latest Chinese satellite in Sun synchronous orbit dedicated to weather and climate monitoring, CMA released 24 hours of observations from the principal

instruments on the platform payload. In this study we have provided a preliminary characterisation of data quality for FY-3D microwave instruments, namely, MWTS-2, MWHS-2, and MWRI, in the perspective of their assimilation in NWP systems. FY-3D observations have been compared to the Met Office short range forecasts, along with observations from the previous Chinese platform, FY-3C, carrying identical instruments (apart from MWTS-2 that is out of service) as well as observations from SNPP ATMS and GPM GMI, two well characterised U.S. instruments. A noteworthy aspect of this comparison is that ATMS, MWHS-2, and GMI observations are assimilated into the Met Office system which should result in a closer agreement with the forecast compared to the observations from the instruments on board FY-3D that are used passively.

We have first assessed MWTS-2 background departures and compared them to those of ATMS at equivalent channel frequencies. Because we could not compare FY-3D MWTS-2 with the FY-3C version we have analysed our results in the light of previous assessment studies. The most interesting finding is a close agreement in global background departures with those found on the same day for ATMS. This represents a significant improvement since the temperature sounder on FY-3C was shown to suffer a large cold inter satellite bias attributed to a suboptimal calibration. The difference between FY-3D MWTS-2 and ATMS O-B is within ± 1 K. The remaining bias for FY-3D MWTS-2 is the scan-dependent bias that can reach amplitudes of up to 2 K and affects, to various extents, all channels. Striping noise and biases varying with the scene temperature and air masses have also been detected in line with previous findings related to the instrument on FY-3C. We have also raised concerns regarding the smoothing method employed by CMA to average the instrument raw digital counts that leads to an increase in striping noise and causes a 0.2-0.5 K bias between the ascending and descending nodes. This method was originally used for FY-3C MWTS-2 but was revised by CMA a few months after launch, which led to a data quality improvement for the instrument on FY-3C and therefore we recommend that it should be revised for the instrument on FY-3D as well.

The assessment of FY-3D MWHS-2 and comparison with the FY-3C version and ATMS at equivalent channel frequencies has revealed a shift in global biases, likely due to a different calibration with respect to the FY-3C version. This shift results in a reduction of the global biases in the 183 GHz humidity channels and places FY-3D MWHS-2 within ± 2.6 K to ATMS O-B. Like the instrument on FY-3C, the new MWHS-2 shows the signs of spurious sensitivity to the instrument environment temperature in channel 14 and, to a lesser extent channel 13, possibly linked to an emissivity leakage affecting the antenna. In the 118 GHz channels, the global bias shift has a detrimental effect, although FY-3D calibration provides a more coherent channel-to-channel bias structure than FY-3C. The standard deviation in O-B is found similar albeit up to 0.6 K larger than the other two instruments. Consistent with previous evaluations of FY-3C MWHS-2, we have detected the presence of striping noise, visible in the 118 GHz, and air mass dependent biases. The bias change with scene temperature appears relatively insignificant but this must be confirmed by the analysis of a larger data set.

From the evaluation of FY-3D MWRI, we have highlighted a reduction of the global biases across most channels as well as a reduction of the standard deviation in O-B compared to the FY-3C version. The latter is consistent with the bias correction developed by CMA aimed at reducing the noise in the warm target used for the calibration. Compared to GMI, the new MWRI is biased low at 10 and 36 GHz but shows better agreement at 18, 23, and 89 GHz where the difference in O-B is generally less than 0.7 K. Focusing on the solar-dependent bias that was found to be as large as 2 K for the instrument on FY-3C and a serious drawback for use in NWP systems, we have shown that this bias has been reduced to less than 0.2 K for FY-3D MWRI (slightly larger in channel 1 and 2 possibly due to sampling effects). This is also the direct result of an improved correction applied by CMA targeting the emissivity of the cold and hot reflectors. It is hoped that CMA will also apply the emissivity correction to the instrument on FY-3C.

In conclusion, this preliminary study has demonstrated very encouraging results with an overall improvement of the data quality from FY-3D instruments with respect to their predecessors. The new set of microwave instruments that FY-3D offers is expected to further strengthen and increase resiliency of the microwave branch of the observing system used for numerical weather predictions, reduce forecast errors, and be more straightforward to use thanks to the mitigation of serious issues affecting past instruments. We also hope that CMA will answer the concerns raised in this paper and that more data will be provided to the community for a more extensive validation.

Acknowledgments

This work was supported by the UK–China Research & Innovation Partnership Fund through the Met Office Climate Science for Service Partnership (CSSP) China as part of the Newton Fund.

References

Atkinson, N., Lu, Q., Bell, B., Carminati, F., Lean, K., Bormann, N. and Lawrence, H.: The FY-3C evaluation project: microwave sounder calibration and direct broadcast experiences, ITSC proceeding https://cimss.ssec.wisc.edu/itwg/itsc/itsc20/papers/1_02_atkinson_paper.pdf, 2015.

Bauer, P., Thorpe, A. and Brunet, G.: The quiet revolution of numerical weather prediction, Nature, 525, 47–55, https://doi.org/10.1038/nature14956, 2015.

Bell, W., Candy, B., Atkinson, N., Hilton, F., Baker, N., Bormann, N., Kelly, G., Kazumori, M., Campbell, W.F., and Swadley S.D.: The assimilation of SSMIS radiances in numerical weather prediction models, IEEE Trans. Geoscience. Rem. Sensing., 46:884 – 900, DOI: 10.1109/TGRS.2008.917335, 2008.

Bennartz, R., Thoss, A., Dybbroe, A., and Michelson D. B.: Precipitation analysis using the advanced microwave sounding unit in support of nowcasting applications, Meteorological Applications, vol. 9, no. 2, pp. 177–189, https://doi.org/10.1017/S1350482702002037, 2002.

Booton, A., Bell, W., and Atkinson, N.: An improved bias correction for SSMIS, ITSC Proceedings, https://cimss.ssec.wisc.edu/itwg/itsc/itsc19/program/papers/10_03_booton.pdf, 2014.

Bormann, N., Fouilloux, A. and Bell, W.: Evaluation and assimilation of ATMS data in the ECMWF system, Journal of Geophysical Research: Atmospheres, 118(23), https://doi.org/10.1002/2013JD020325, 2013.

Brogniez, H., English, S., Mahfouf, J.F., Behrendt, A., Berg, W., Boukabara, S., Buehler, S.A., Chambon, P., Gambacorta, A., Geer, A. and Ingram, W.,: A review of sources of systematic errors and uncertainties in observations and simulations at 183GHz, Atmospheric Measurement Techniques, 9(5), pp.2207-2221, DOI : 10.5194/amt-9-2207-2016, 2016.

Calbet, X., Peinado-Galan, N., DeSouza-Machado, S., Kursinski, E. R., Oria, P., Ward, D., Otarola, A., Rípodas, P., and Kivi, R.: Can turbulence within the field of view cause significant biases in radiative transfer modelling at the 183 GHz band?, Atmos. Meas. Tech. Discuss., https://doi.org/10.5194/amt-2018-181, in review, 2018.

Carminati, F., Goddard, J., Lawrence, H., Newman, S.: Calibration/validation study of GPM GMI, GAIA-CLIM Delivrable D4.6, http://www.gaia-clim.eu/system/files/document/d4.6.pdf, 2017.

Carminati, F., Candy, B., Bell, W., and Atkinson, N.: Assessment and assimilation of FY-3 humidity sounders and imager in the UK Met Office global model. Adv. Atmos. Sci., 35(8), 942–954, https://doi.org/10.1007/s00376-018-7266-8, 2018.

Carminati, F., Migliorini, S., Ingleby, B., Bell, W., Lawrence, H., Newman, S., Hocking, J., and Smith, A.: Using reference radiosondes to characterise NWP model uncertainty for improved satellite calibration and validation, Atmos. Meas. Tech. Discuss., https://doi.org/10.5194/amt-2018-219, in review, 2018.

Chen, K., English, S. J., Bormann, N., and Zhu, J.: Assessment of FY-3A and FY-3B MWHS observations, Wemher Forecast, vol. 30. pp. 1280-1290, https://doi.org/10.1175/WAF-D-15-0025.1, 2015.

Chen, K. Y., Bormann, N., English, S., and Zhu, J.: Assimilation of Feng-Yun-3B satellite microwave humidity sounder data over land, Adv. Atmos. Sci., 35(3), 268–275, https://doi.org/10.1007/s00376-017-7088-0, 2018.

English, S. J., Eyre J. R., and Smith, J. A.: A cloud-detection scheme for use with satellite sounding radiances in the context of data assimilation for numerical weather prediction, Quarterly Journal of the Royal Meteorological Society, vol. 125, no. 559,pp. 2359–2378, https://doi.org/10.1002/qj.49712555902, 1999.

English, S. J., Renshaw, R. J., Dibben, P. C., Smith, A. J., Rayer, P. J., Poulsen, C. , Saunders, F. W. and Eyre, J. R.: A comparison of the impact of TOVS arid ATOVS satellite sounding data on the accuracy of numerical weather forecasts, Q.J.R. Meteorol. Soc., 126: 2911-2931, doi:10.1002/qj.49712656915, 2000.

Geer, A.J., Bauer, P., and Bormann, N.: Solar biases in microwave imager observations assimilated at ECMWF. IEEE Trans. Geoscience. Rem. Sensing, 48:2660–2669, DOI: 10.1109/TGRS.2010.2040186, 2010.

Jieying, H., Shengwei, Z. and Zhenzhan, W.: Advanced microwave atmospheric sounder (AMAS) channel specifications and T/V calibration results on FY-3C satellite, IEEE Transactions on Geoscience and Remote Sensing, 53(1), pp.481-493, DOI: 10.1109/TGRS.2014.2324173, 2015.

Joo, S., Eyre, J., and Marriott, R.: The Impact of MetOp and Other Satellite Data within the Met Office Global NWP System Using an Adjoint-Based Sensitivity Method, Mon. Wea. Rev., 141, 3331–3342, https://doi.org/10.1175/MWR-D-12-00232.1, 2013.

Kazumori, M. and English, S. J.: Use of the ocean surface wind direction signal in microwave radiance assimilation, Q.J.R. Meteorol. Soc., 141: 1354–1375, https://doi.org/10.1002/qj.2445, 2015.

Kazumori, M., Geer, A. J., and English, S. J.: Effects of all-sky assimilation of GCOM-W/AMSR2 radiances in the ECMWF numerical weather prediction system, Q.J.R. Meteorol. Soc., 142: 721-737, doi:10.1002/qj.2669, 2016.

Kim, E., Lyu, C.-H. J., Anderson, K., Leslie, R. V., and Blackwell, W. J.: S-NPP ATMS instrument prelaunch and on-orbit performance evaluation, J. Geophys. Res. Atmos., 119, 5653–5670, doi: 10.1002/2013JD020483, 2014.

Lawrence, H., Carminati, F., Bell, W., Bormann, N., Newman, S., Atkinson, N., Geer, A., Migliorini, S., Lu, Q. and Chen, K.: An Evaluation of FY-3C MWRI and Assessment of the long-term quality of FY-3C MWHS-2 at ECMWF and the Met Office. European Centre for Medium-Range Weather Forecasts, https://www.ecmwf.int/sites/default/files/elibrary/2017/17206-evaluation-fy-3c-mwri-and-assessment-long-term-quality-fy-3c-mwhs-2-ecmwf-and-met-office.pdf, 2017.

Lawrence, H., Bormann, N., Geer, A.J., Lu, Q. and English, S.J.: Evaluation and Assimilation of the Microwave Sounder MWHS-2 Onboard FY-3C in the ECMWF Numerical Weather Prediction System, IEEE Transactions on Geoscience and Remote Sensing, 56(6), pp.3333-3349, DOI:10.1109/TGRS.2018.2798292, 2018.

Li, J., Qin, Z., Liu, G.: A new generation of Chinese FY-3C microwave sounding measurements and the initial assessments of its observations, International Journal of Remote Sensing, 37:17, 4035-4058, DOI: 10.1080/01431161.2016.1207260, 2016.

Li, J. and Liu, G.: Direct assimilation of Chinese FY-3C Microwave Temperature Sounder-2 radiances in the global GRAPES system, Atmos. Meas. Tech., 9, 3095-3113, https://doi.org/10.5194/amt-9-3095-2016, 2016.

Li, J. and Liu, G.: Assimilation of Chinese FengYun 3B Microwave Temperature Sounder radiances into Global GRAPES system with an improved cloud detection threshold, Front. Earth. Sci., 10, 145–158, doi:10.1007/s11707-015-0499-2, 2015.

Li, J. and Zou, X.: Impact of FY-3A MWTS radiances on prediction in GRAPES with comparison of two quality control schemes, Front. Earth. Sci., 8, 251–263, doi:10.1007/s11707-014-0405-3, 2014.

Lu, Q. F., Bell, W., Bauer, P., Bormann, N., and Peubey, C.: Characterizing the FY-3A microwave temperature sounder using the ECMWF model, J. Atmos. Oceanic Technol., 28(11), 1373–1389, https://doi.org/10.1175/JTECH-D-10-05008.1, 2011.

Lu, Q. F., Lawrence, H., Bormann, N., English, S., Lean, K., Atkinson, N., Bell, W., and Carminati, F.: An evaluation of FY-3C satellite data quality at ECMWF and the Met Office, European Centre for Medium-Range Weather Forecasts Tech. Memo., 767, https://www.ecmwf.int/sites/default/files/elibrary/2015/14692-evaluation-fy-3c-satellite-data-quality-ecmwf-and-met-office.pdf, 2015.

Lorenc, A. C., Ballard, S. P., Bell, R. S., Ingleby, N. B., Andrews, P. L., Barker, D. M., Bray, J. R., Clayton, A. M., Dalby, T. , Li, D. , Payne, T. J. and Saunders, F. W.: The Met. Office global three-dimensional variational data assimilation scheme, Quarterly Journal of the Royal Meteorological Society, 126: 2991-3012, doi:10.1002/qj.49712657002, 2000.

Newell, D., Draper, D., Figgins, D., Berdanier, B., Kubitschek, M., Holshouser, D., Sexton, A., Krimchansky, S., Wentz, F. and Meissner, T.: GPM microwave imager key performance and calibration results, In Geoscience and Remote Sensing Symposium (IGARSS), IEEE International, pp. 3754-3757, DOI: 10.1109/IGARSS.2014.6947300, 2014.

Newell, D., Draper, D., Remund, Q., Figgins, D., Krimchansky, S., Wentz, F. and Meissner, T.: GPM Microwave Imager (GMI) on-orbit performance and calibration results, In Geoscience and Remote Sensing Symposium (IGARSS), IEEE International, pp. 5158-5161, DOI:10.1109/IGARSS.2015.7326995, 2015.

Pielke, R., and Carbone, R.E.: Weather impacts, forecasts, and policy, Bull. Amer. Meteor. Soc., 83, 393–406, https://doi.org/10.1175/1520-0477(2002)083<0393:WIFAP>2.3.CO;2, 2002.

Rawlins, F., Ballard, S., Bovis, K., Clayton, A., Li, D., Inverarity, G., Lorenc, A., and Payne, T.: The Met Office global four-dimensional variational data assimilation scheme, Quarterly Journal of the Royal Meteorological Society, 133: 347-362, doi:10.1002/qj.32, 2007.

Saunders, R. W., Blackmore, T. A., Candy, B., Francis, P. N., and Hewison, T. J.: Monitoring satellite radiance biases using NWP models, IEEE Trans. Geosci. Remote Sens., 51(3),1124–1138, https://doi.org/10.1109/TGRS.2012.2229283, 2013.

Saunders, R., Hocking, J., Turner, E., Rayer, P., Rundle, D., Brunel, P., Vidot, J., Rocquet, P., Matricardi, M., Geer, A., Bormann, N., and Lupu, C.: An update on the RTTOV fast radiative transfer model (currently at version 12), Geosci. Model Dev. Discuss., https://doi.org/10.5194/gmd-2018-64, 2018.

Tian, X., Zou, X., and Yang, S.: A limb correction method for the Microwave Temperature Sounder 2 and its applications, Adv. Atmos. Sci., 35(12), 1547–1552, https://doi.org/10.1007/s00376-018-8092-8, 2018.

Uppala, S. M., KÅllberg, P. W., Simmons, A. J., Andrae, U. , Bechtold, V. D., Fiorino, M. , Gibson, J. K., Haseler, J. , Hernandez, A. , Kelly, G. A., Li, X. , Onogi, K. , Saarinen, S. , Sokka, N. , Allan, R. P., Andersson, E. , Arpe, K. , Balmaseda, M. A., Beljaars, A. C., Berg, L. V., Bidlot, J. , Bormann, N. , Caires, S. , Chevallier, F. , Dethof, A. , Dragosavac, M. , Fisher, M. , Fuentes, M. , Hagemann, S. , Hólm, E. , Hoskins, B. J., Isaksen, L. , Janssen, P. A., Jenne, R. , Mcnally, A. P., Mahfouf, J. , Morcrette, J. , Rayner, N. A., Saunders, R. W., Simon, P. , Sterl, A. , Trenberth, K. E., Untch, A. , Vasiljevic, D. , Viterbo, P. and Woollen, J.: The ERA-40 re-analysis, Q.J.R. Meteorol. Soc., 131: 2961-3012, doi:10.1256/qj.04.176, 2005.

Wang, Z., Li, J., He, J., Zhang, S., Gu, S., Li, Y., Guo, Y. and He, B.: Performance Analysis of Microwave Humidity and Temperature Sounder Onboard the FY-3D Satellite From Prelaunch Multiangle Calibration Data in Thermal/Vacuum Test, IEEE Transactions on Geoscience and Remote Sensing, DOI: 10.1109/TGRS.2018.2868324, 2018.

Wang, X., Li, X.: Preliminary investigation of FengYun-3C Microwave Temperature Sounder (MWTS) measurements, Remote Sensing Letters, 5:12, 1002-1011, DOI: 10.1080/2150704X.2014.988305, 2014.

Xingfa, G., and Xudong, T.: Overview of China Earth Observation Satellite Programs [Space Agencies], in IEEE Geoscience and Remote Sensing Magazine, vol. 3, no. 3, pp. 113-129, doi: 10.1109/MGRS.2015.2467172, 2015.

Yang, W.; John, V.O.; Zhao, X.; Lu, H.; Knapp, K.R: Satellite Climate Data Records: Development, Applications, and Societal Benefits, Remote Sens., doi:10.3390/rs8040331, 2016.

Yang, Z., Lu, N., Shi, J., Zhang, P., Dong, C., and Yang, J. :Overview of FY-3 Payload and Ground Application System, in IEEE Transactions on Geoscience and Remote Sensing, vol. 50, no. 12, pp. 4846-4853, doi: 10.1109/TGRS.2012.2197826, 2012.

Yang, H., Weng, F., Lv, L., Lu, N., Liu, G., Bai, M., Qian, Q., He, J. and Xu, H.: The FengYun-3 microwave radiation imager on-orbit verification, IEEE Transactions on Geoscience and Remote Sensing, 49(11), pp.4552-4560, DOI: 10.1109/TGRS.2011.2148200, 2011.

Zou, X., Wang, X., Weng, F. and Li, G.: Assessments of Chinese Fengyun Microwave Temperature Sounder (MWTS) measurements for weather and climate applications, Journal of Atmospheric and Oceanic Technology, 28(10), pp.1206-1227 https://doi.org/10.1175/JTECH-D-11-00023.1, 2011.

Zou, X., Zhao, J., Weng, F. and Qin, Z.: Detection of radio-frequency interference signal over land from FY-3B Microwave Radiation Imager (MWRI), IEEE Transactions on Geoscience and Remote Sensing, 50(12), pp.4994-5003, DOI: 10.1109/TGRS.2012.2191792, 2012.

Met Office
FitzRoy Road
Exeter
Devon
EX1 3PB
United Kingdom